Design, simulation and experiments for direct thixotropic metal 3D printing

Yifan Fei¹, Jie Xu¹, Donggang Yao², Richard Chiou³, Jack Zhou^{1,*}

¹Department of Mechanical Engineering and Mechanics, Drexel University, Philadelphia, PA, USA

²School of Materials Science and Engineering, Georgia Institute of Technology, Atlanta, GA, USA.

³Department of Engineering Technology, Drexel University, Philadelphia, PA, USA

^{*} Correspondence to: Jack Zhou, Department of Mechanical Engineering and Mechanics, Drexel University, PA, USA; Zhoug@drexel.edu.

Design, simulation and experiments for direct thixotropic metal 3D printing

Abstract

Compared with current powder based 3D metal printing, thixotropic metal 3D printing has great potentials and advantages in equipment cost, product quality and process efficiency. In this paper, detailed problem statement, technique challenge, and development method regarding thixotropic metal 3D printing have been discussed. A shear mixing and extruding prototype machine for thixotropic alloy fabrication has been designed. A direct thixotropic metal 3D printing machine has been developed and a modeling and simulation process for the system has been conducted. The printability of this direct metal 3D printing machine has been studied. At the end, conclusions and future directions are also presented.

Keywords: Thixotropic 3D printing; Thixotropy; Semi-solid metal; Semi-solid metal processing; Direct metal printing

1. Introduction

For traditional metals such as titanium and stainless steel, laser melting/sintering of powders is a typical additive manufacturing (AM) process. However, laser melting/sintering, not mentioning its slow and expensive process, is technically not suitable for chemically reactive metal powers such as Al, Mg and Zn powders because these powers under normal conditions are covered naturally by a passivated oxidation layer. Al, Zn and Mg are low-melting-point metals (660°C, 519.5°C and 650°C, respectively), but their oxides have melting temperature close to 2000°C or even higher. The high laser energy needed to break the oxides leads to poor fusion quality caused by undesired metallurgical defects such as porosity, cracking, and evaporation of alloying elements [1]. Likewise, other powder-based binding (e.g., using an organic binder) and sintering processes are also not suitable for processing Al, Mg and Zn alloys into precision parts with high fusion quality.

Ideally, liquid-state deposition by jetting or by extrusion is highly desired in additive manufacturing of low-melting-point Al, Mg and Zn alloys. Currently, almost all commercially available jetting/extrusion machines rely on a binder material to formulate a printable compound for metallic materials. One major drawback of exists method is additional post-printing process such as debinding and sintering. In jetting, droplets of building material are formed by capillary breakup and selectively deposited on substrate; by comparison, in extrusion, material is extruded as a liquid thread and deposited on substrate (according to ISO/ASTM 52900 Standard) [2]. In recent years, the material extrusion technique has already been evolved into a mature technique for several other materials such as polymer, composites, hydrogel, etc.[3-5]. However, liquid-state deposition of molten metal with accuracy suitable for additive manufacturing remains to be an immense challenge [6, 7]. The difficulty arises from the unfavorable rheology of molten metals, that is, extremely low viscosity but exceptionally high surface tension. This leads to uncontrollable coalescence and breakup of the fluid under normal conditions, as such neither controllable droplets nor stable liquid threads can be formed.

1.1 Thixotropic property and semi-solid metal processing

Thixotropy refers to a material's yielding and shear-thinning properties. When the material is sheared, it thins, but when the material is allowed to stand, it thickens again [8]. For a suspension or slurry, this behavior is related to the disintegration of solid particle agglomerates in the presence of shear and their reformation after the shear is removed. For a metallic alloy under cooling, this behavior is observed when the microstructure is composed of solid spheroids suspended in a liquid matrix (Figure 1) [8]. Thixotropy forms the theoretical foundation for semi-solid metal (SSM) processing, and as a results several SSM processing methods have already been developed and commercialized for molding and casting applications. In particular, continuous stirring and extrusion is one popular SSM method for the alloy industry, and thixomolded magnesium alloy has become one of the major products for light-weight structural applications including components for automotive.

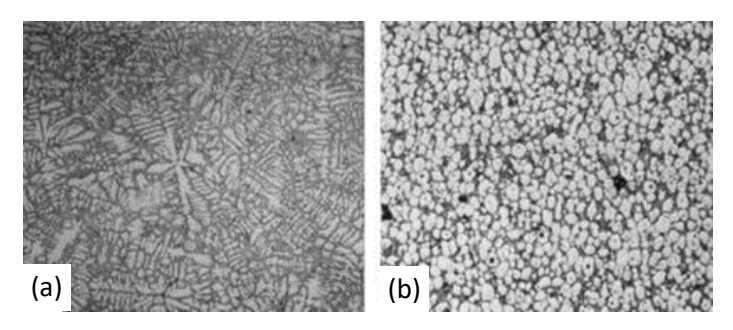


Fig. 1. Microstructure of solidified alloy: (a) dendritic microstructure in an as-cast sample; and (b) a globular microstructure in a semisolid alloy sample [8].

1.2 Problem Statement

Liquid-state deposition by jetting or by extrusion represents the most cost-effective and successful techniques in additive manufacturing [9]. In jetting, liquid droplets are created while in extrusion, a liquid filament is generated. Jetting-based and extrusion-based machines share many common features in design, and both are simple compared with beam-based melting/sintering machines. 3D printing machines are now widely available from leading manufacturers including 3D System, Stratasys, XJET, HP, Voxeljet, ExOne, Desktop, and Prodways. They can be divided into two groups: direct deposition and binder deposition. Nevertheless, for metallic materials, all commercially available jetting/extrusion machines rely on a binder material (mostly organic materials) for formulating a printable compound; direct printing of molten metal for controllable freeform 3D fabrication has not yet been achieved.

This difficulty in liquid-state deposition of molten metal is understandable by examining the Ohnesorge number, Oh, defined as a ratio of viscous force over the combined inertia and surface tension forces,

$$Oh = \mu / \sqrt{\rho \sigma L} \tag{1}$$

where μ is viscosity, ρ is density, σ is surface tension, and L is characteristic size. For molten metal, the surface tension is typically about several 100s of mN/m, while the viscosity is very low, about a few centipoises (mPa·s). For a 0.1 mm sized droplet, the Oh number is calculated to

be on the order of 0.005 (assuming $\rho \approx 5000$ Kg/m³). For jetting of droplets, the needed Oh number is typically in the range of 0.1 to 1 [10, 11]. On the other hand, for stable formation of a liquid filament, a larger Oh number much greater than 1 is needed. It then becomes apparent that neither droplets nor filaments as desired in 3D printing can be formed in a stable, controllable manner for molten metal. Actually, molten metal is extremely hard to harness under normal extrusion conditions [6, 7]; the ultrahigh surface tension dictates instability such as coalescence and breakup, especially sensitive to process variations and local geometrical changes. The large surface tension also makes adhesion to the substrate difficult. As such, **currently there exists an immense difficulty in liquid-state deposition/printing of molten metal.**

From perspectives of fluid physics, the surface tension in general is not easy to modify, but the viscosity is. Therefore, one may increase the viscosity (or flow resistance forces) so that the Oh number becomes sufficiently large for filament formation. Actually, some limited work [7, 12] has been conducted to improve filament formation of liquid metal by increasing flow resistance, e.g., through alloy formulation. However, existing ideas have only generated limited initial results and still remain as scientific subjects to be explored.

For low-melting and chemically reactive alloys such as Al, Zn and Mg based alloys, enabling direct extrusion is of a particular significance, since powder-based fusion processes do not work well for these alloys due to the passivation layer [1]. Cost-effective printing of these alloys would lead to a revolutionary improvement on the products of medical devices, engineering and industrial product and beyond. Therefore, a new technical approach for breaking the physical limit set by an extremely low Ohnesorge number of molten alloy and enabling direct printing is highly desired.

1.3 Manufacturing Process and System Development

The main objective of this research is to explore a novel manufacturing system that is capable of thixotropically processing and 3D printing of low melting point alloys such as Al, Mg, Zn alloys into various devices and products. To enable direct extrusion of molten metal, one has to find a practically viable approach for substantially increasing the Ohnesorge number. From Eq. (1)), this requires increasing of viscosity or decreasing of surface tension. Therefore, one has to modify the material properties of the liquid metal by increasing the flow stress and decreasing the negative effects from the high surface tension. In this paper, some low melting point alloys were made into a thixotropic fluid, like a toothpaste, having a desired non-Newtonian fluid property for direct extrusion. A thixotropic fluid is characterized with a high viscosity and a yield stress at a low strain rate, but the fluid thins at increasing strain rate. Inside the nozzle, the viscosity is low because of high shear rate, so flow is enabled. Outside the nozzle, the shear rate rapidly vanishes, so a yield stress is produced to counterbalance the surface tension. This thixotropy not only permits the printing fluid to form a stabilized paste-like filament during printing and furthermore allows the printed fluid not to sag in the absence of a mold, thus enabling direct 3D printing with high geometrical control.

Thixotropy is not completely new in alloy processing. Actually, near net-shape manufacturing processes by semisolid processing are currently available, including thixocasting, rheocasting and thixomolding [13-15]. Semisolid processing has several advantages [13]: 1. The capital investment and operating costs is significantly lower compared with conventional casting methods. The whole process can be contained within one machine so that the need for melting and holding furnaces as well as melt treatment are all avoided. Foundry cleanliness is easy to

maintain, and energy requirements are less because complete melting is not required, cycle times are reduced, and scrap is minimized. 2. Shrinkage and cracking within the mold are reduced because the alloy is already partly solidified in cast. 3. Lower operating and pouring temperatures lead to an increase in the life of metal dies. 4. Composite materials can be readily produced by adding microspheres, fibers or other solid particulates into the feedstock (often referred to as compo casting). Despite these advantages, all existing processes need a mold for shaping. The thixotropy generated in existing processes is considered not adequate and suitable for 3D printing. The solid inclusions in these processes are large in size and irregular in shape, often containing large dendritic structures. In this research, a mixer was designed for producing a printable micro-slurry from metallic alloys. The desired micro-slurry should a two-phase structure, containing a fine β -phase grains (of a high melting point) uniformly dispersed in a molten α -phase. This micro-slurry is then directly fed into a filament extruder for 3D printing, as illustrated in Fig. 2. For demonstration purposes, several low-melting-point alloys were chosen in the experimental work in this study.

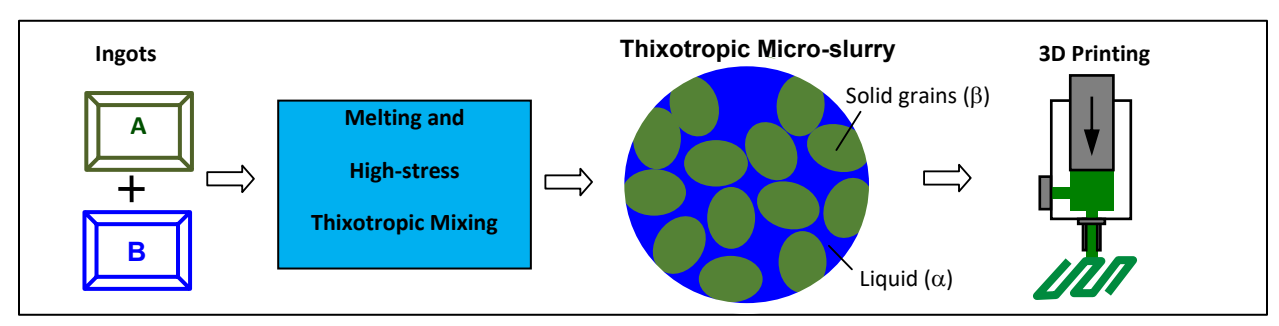


Fig. 2. Process design for thixotropic shearing-mixing and 3D printing of alloy with a dispersed grain structure.

2. Equipment Design

2.1 Thixotropic metal extruder design

The core part of the thixotropic metal extruder was designed in conjunction with the following components (Figure 3): motor and gearbox, auger bit, hopper, material transfer channel, heating elements, and nozzle. The body of the extruder was modified by a Filabot EX2 polymer filament extruder. The heating system comprise three sections: a high-temperature region for material melting, a low-temperature region for semi-solid formation, and a nozzle reheat region. The region of high-temperature heating is located near the material feeding hopper. When raw material pellets are inserted into the machine, the bit transports them to the heating region. This section's heating temperature is slightly higher than the material's melting point. The purpose of establishing a high temperature in this section is to melt or soften the raw material. Dual element heating tape (from Omega Engineering) is chosen as a heating element in high-temperature heating regions. This heating tape has a maximum heating temperature of 1400°F (760°C), which is suitable for the majority of low melting metals. Alternatively, the heating element can be replaced with an induction heater so that the metal melts while simultaneously generating globular microstructure. The region of low-temperature heating is equipped with a fiberglass heating rope (from Omega Engineering) capable of producing heat up to 900°F (482°C). The material in this section is cooled and sheared as the auger bit rotates.

When the temperature decreases, the molten metal begins to transition from the liquid to the solid phase. The shearing action within the channel aids in grain size reduction and the formation of near-globular grains. After passing through the low-temperature section, the processed material is reheated and squeezed out through the nozzle to form small beads. The nozzle is connected to a band heater in this section to maintain a constant heating temperature. With reheating, a semi-solid slurry's solid fraction is reduced, and the material's viscosity is decreased for easy flow.

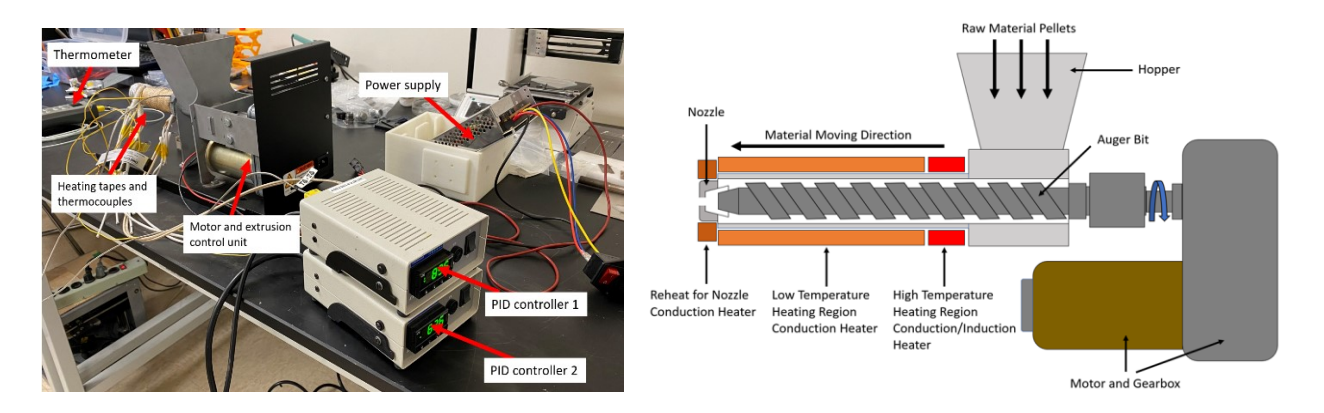


Fig. 3. Illustration of the components in the thixotropic metal extruder.

2.2 Thixotropic printing system design

The thixotropic printing system is composed of an extrusion printing nozzle mounted on a support frame that also houses the reservoir and extrusion mechanism. Figure 4 illustrates the frame design and the major controlling system mounted on it. The frame is supported by steel struts and features an adjustable central holding area for the reservoir. A motion controller controls an electric linear actuator (IP66 series from Progressive Automations) that moves at a speed of 3.8 mm/s – 38.1 mm/s. Three control systems are incorporated into the design. Through the extrusion motion controlling system, the actuator and motion controller are connected. The controller can adjust the extrusion speed to the extrusion requirements of the material. The temperature PID control system consists of two heating regions. Both heating regions are controlled by a benchtop PID controller (from Omega Engineering). According to the measurements, the actual temperature received inside the channel is on average 5°C less than the PID setup temperature. As a result, the input temperature for heat tape 1 is set to 78°C, while the input temperature for heat tape 2 is set to 69°C. Due to the fact that the printing material is produced as pellets, the melting rate is significantly faster than with a conventional ingot. The auger bit rotates at a speed of 60 rpm, depending on the melting condition of the material. An alloy processed by the extruder is extruded out as a semi-solid slurry using 1mm-1.5mm outlet nozzle. The material is printed on the substrate as a result of gravity and extrusion force.

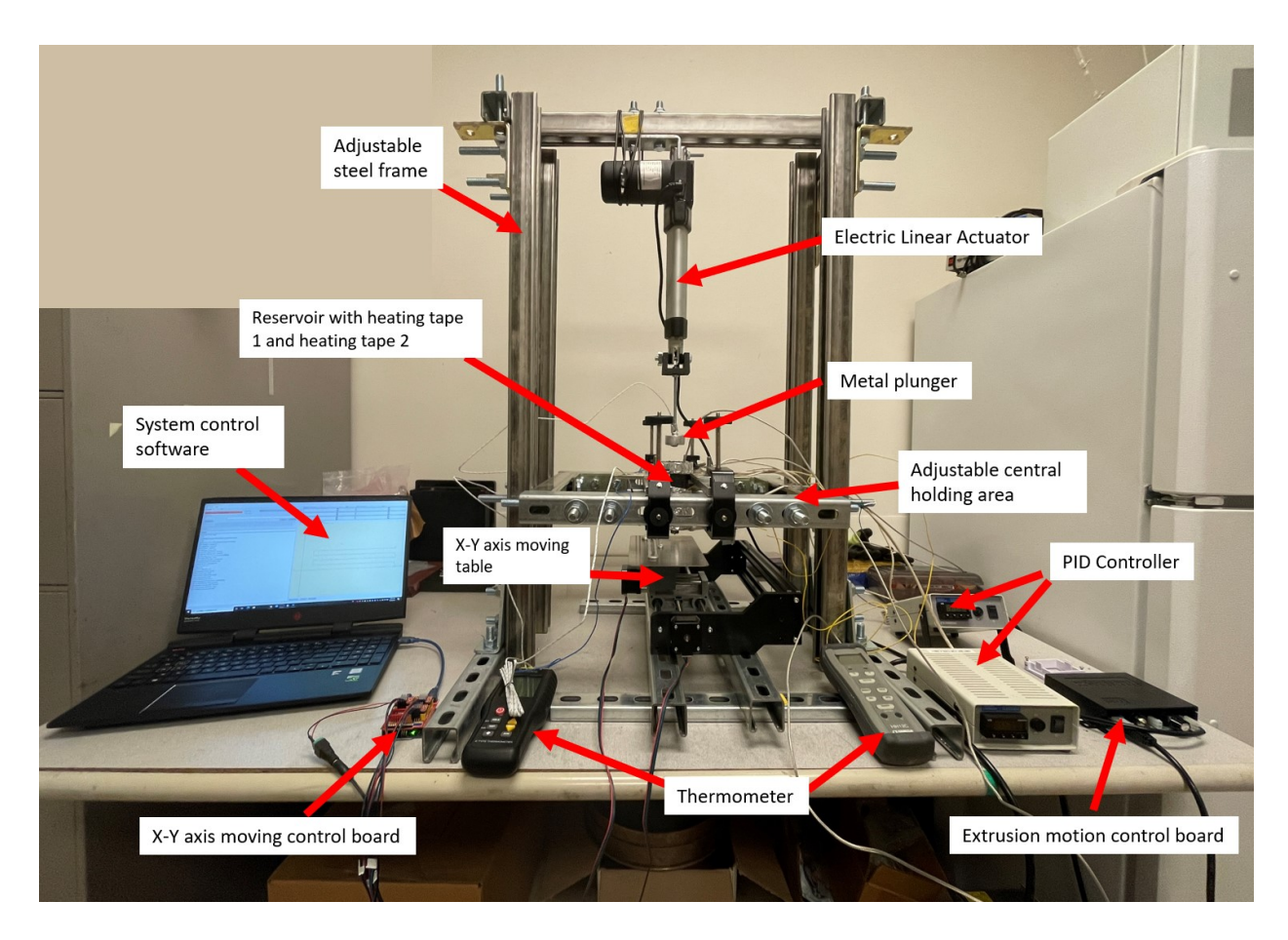
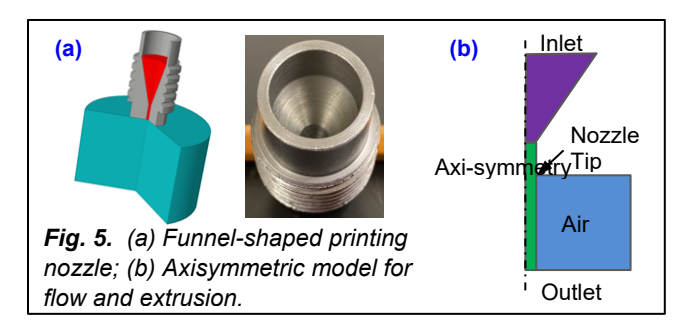


Fig. 4. Plunger extrusion based printing system design

3. Simulation and Prediction

3.1 Modeling and Simulation of Thixotropic Metal 3D Printing



Computer simulations were conducted to study the free surface flow during extrusion and 3D printing. A funnel-like nozzle is used in the geometrical model, as shown in Fig. 5a. The funnel has entry and exit diameters of 40 mm and 2 mm. The free-surface flow is modeled in an axisymmetric 2D domain (Fig. 5b). A thixotropic metal slurry enters the funnel from the inlet and then flows out of

the nozzle tip to evolve into a free-surface flow surrounded by air. Surface tension is applied at the slurry to air interface. The rheological properties (including yield stress and viscosity) of a thixotropic fluid is supposed to depend on the solid fraction and structure. In this preliminary study, only the effect of variable viscosity of the thixotropic fluid was considered, leading to a variable Ohnesorge number (Eq.1)). The density is set to a representative values of 4000 Kg/m³. For the nozzle size of 2 mm, the Oh number used in the simulation ranges from 0.001 to 1000. In moving boundary flow simulation, the free surface is often tracked using the level set method or

the phase field method. In this preliminary study, the level set method is used, where the interface is tracked by a level set function ϕ governed by

$$\frac{d\phi}{dt} + \gamma \left[\nabla \cdot \left(\phi (1 - \phi) \frac{\nabla \phi}{|\nabla \phi|} \right) - \varepsilon \nabla^2 \phi \right] = 0$$
 (2)

where t is time, and γ and ε are parameters controlling numerical convergence. A similar method has previously been used by others to simulate inkjet printing and channel flow of thixotropic fluids [16, 17].

As an example, some simulation results about the effect of the Oh number on the flow front displacement are provided here. The Weber number (defined as We = $\rho u^2 L/\sigma$ where u is velocity) is set constant at We = 0.018. As shown in Fig. 6, for a low Oh number (e.g., Oh = 0.167), the flow front is leveled off as time increases. This indicates that continuous extrusion is not possible at low Oh number or low viscosity. On the contrary, at higher Oh number (corresponding to high viscosity), the flow front continuously penetrate forward. The simulation also show that the flow front moves slower at a high Oh number, and the diameter of the extruded filament becomes larger (see Fig. 7 for a snapshot). This can lead to a stable filament extrusion process at high Oh number. In fact, the preliminary experimental work also showed that a thixotropic fluid with a high viscosity is highly controllable during printing and the extruded filaments can be readily deposited on the printing platform.

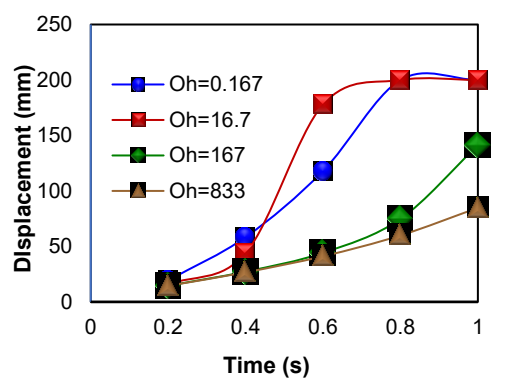


Fig. 6. Flow front displacement for varied Oh number. The We number is fixed at 0.018.

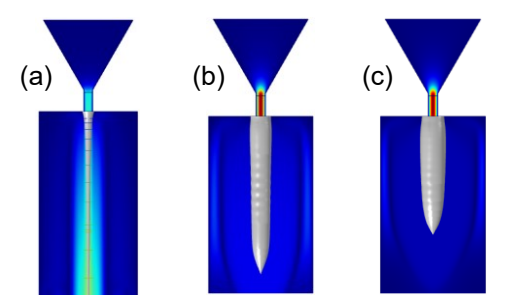


Fig. 7. Thixotropic fluid interface at (a) Oh=0.0167, (b) Oh=167 and (c) Oh=833.

The simulation results presented above are rather preliminary, and yet demonstrate the importance of viscosity in affecting the extrusion and printing process.

3.2 Simulation for material liquid fraction and temperature distribution

The purpose of simulation within the reservoir is to determine the liquid fraction of material contained within the reservoir when the desired heating source is used. In this simulation, a simplified reservoir with an integrated 1mm diameter nozzle is adopted, and a Bi-Pb alloy is used as a material. It is assumed that the alloy would remain stable within the reservoir. The heating source is defined to cover a specific boundary region of the reservoir. The geometry configuration is depicted in Fig. 8(a). The boundary conditions of the two-dimensional cross-sectional view are shown in Fig.8(b). Both top and bottom of the reservoir are defined as the boundary of air. Both air and the outer boundary are assumed to be at ambient temperature (20°C).

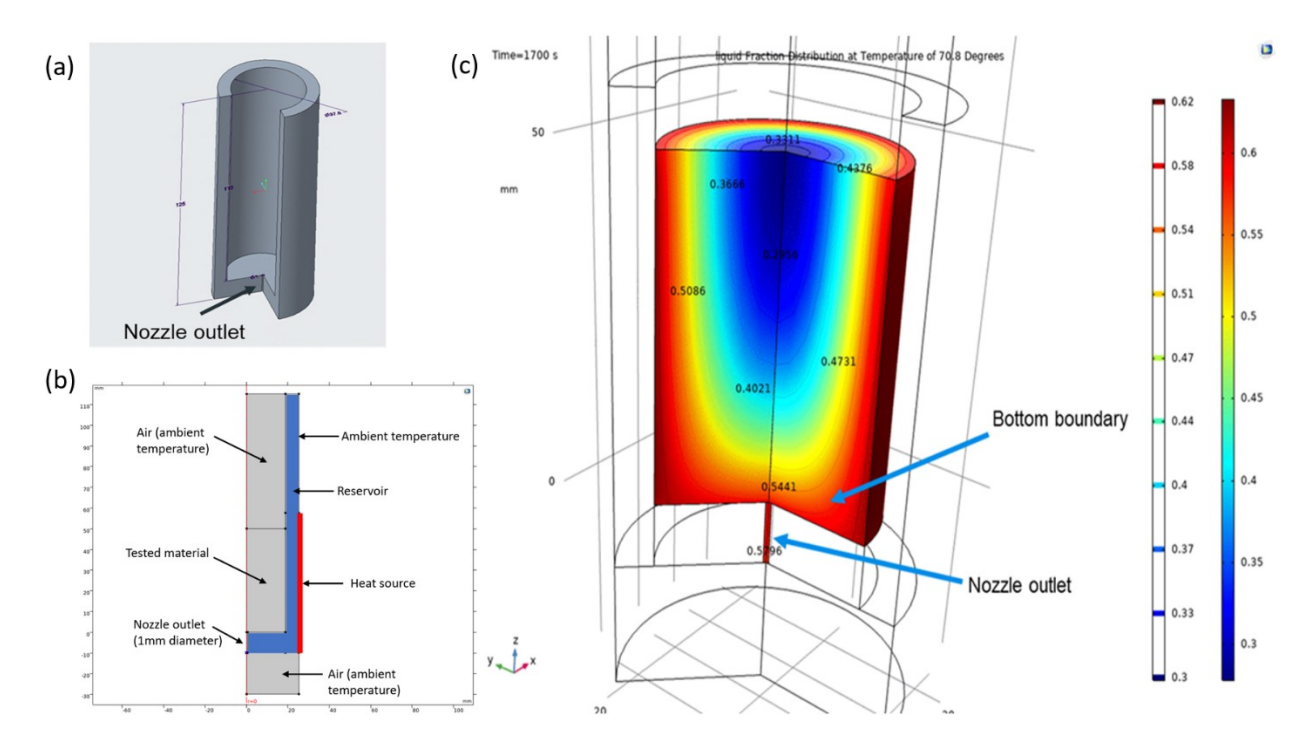


Fig. 8. (a) Simulation model of the reservoir; (b) Cross-sectional area of simulated domain with boundary conditions. A heat source is located at the outer boundary of the reservoir, (c) Liquid fraction distribution within the reservoir for setup temperature of 70.8°C.

The major factor in this simulation is liquid fraction. The general liquid fraction can be defined according to Ref. [17, 18] as

$$f_{l} = \left(\frac{T_{m} - T}{T_{m} - T_{l}}\right)^{\frac{1}{k_{p} - 1}} \tag{3}$$

where T_m is melting point of the solid phase, T_L is liquidus temperature of the low-melting-temperature phase, and k_p is equilibrium partition coefficient.

A Bi-Pb alloy is chosen as a material in the simulation. The corresponding material properties for this alloy are $\sigma = 0.4371 - 0.000066T$ (N/m), $\rho = 11096 - 1.3236T$ (kg/m³), $c_p = 159 - 0.00272T + 7.12(10^{-6})T^2$ (J/kg/K), $\lambda = 3.61 + 0.01517T - 1.714(10^{-6})T^2$ (W/m/K), $T_l = 343$ K, and $\eta = 0.000494 \exp(754.1/T)$ (Pa·s), where ρ is density, c_p is isobaric specific heat, λ is thermal conductivity, and η is dynamic viscosity.

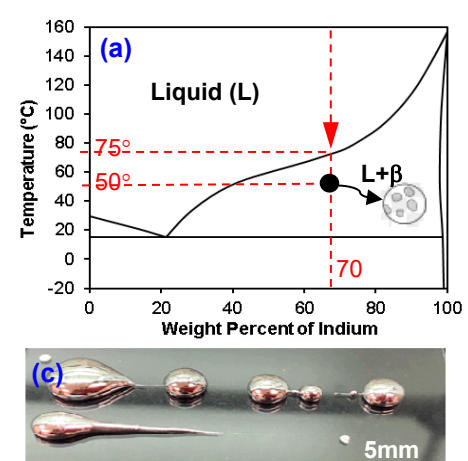
In an ideal estimate, a liquid fraction of around 0.4-0.6 is desired for a semi-solid slurry to become a suitable printing material. When the liquid fraction is less than 0.2, the material is closer to a solid; in contrast, when the liquid fraction is greater than 0.7, the material is closer to a liquid. Temperature and liquid fraction are calculated in this simulation as a function of time over a period of time. The simulation is adjusted to reach a steady state on a time scale of approximately 30 minutes that is comparable to the observed thermal response in the actual experimental observation on the laboratory setup. As illustrated in Figure 8(c), the material around the bottom boundary has a liquid fraction of approximately 0.55 for the 70.8°C test, while the liquid fraction at the nozzle outlet is 0.579.

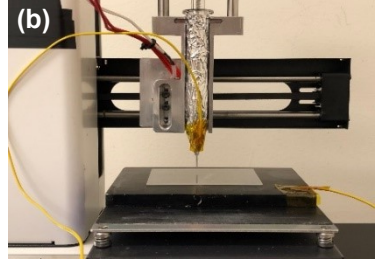
The simulation results indicate that the nozzle region of this Bi-Pb alloy requires accurate temperature control. In this case, the temperature range required to generate the desired material liquid fraction is only 0.51°C. The bottom boundary and the nozzle outlet must have a similar temperature distribution to produce a uniform liquid fraction. Simulated temperature setup and liquid fraction distribution can be used to optimize the heating system design for the printing test. However, the physical setup must take into account the actual heat loss during the heating process and the nozzle attachment. Overall, this reservoir simulation with varying heating temperatures provides in a meaningful prediction tool to guide the design of the experimental setup. In fact, with the aid of the simulation, the heating efficiency was improved and the temperature differential between the PID input and actual heating temperatures was reduced.

4. Experiments

4.1 Initial printing experiments with indium-gallium alloy and bismuth-lead alloy

Due to practical limitations from materials, equipment, and facility, only several alloys with very low melting point were chosen for initial tests. A preliminary study was conducted to test the feasibility of thixotropic alloy as an additive manufacturing material. This section describes the results from an indium-gallium alloy. Indium-gallium alloy is well-known for its electrochemical and rheological properties. Therefore, some researchers have focused on developing electronic circuits and microchannels using In-Ga based alloys [19-21]. Following the In-Ga phase diagram [22-24] (shown in Fig. 9a), it was decided to choose a 70/30 In-Ga composition for testing. From the phase diagram, it is anticipated that when the molten alloy is cooled to about 75°C, a two-phase structure containing a liquid phase and a solid phase would be formed. Specifically, indium was melted at 170°C, and then gallium was added and mixed well at this temperature. The alloy was then gradually cooled to about 50°C while under vigorous mixing. The resulting mixture at 50°C was a paste-like material, able to form sharp shapes when deformed and sustain the deformed shape, indicating formation of a thixotropic fluid. This material was used for 3D printing using a syringe-type printer, as shown in Fig. 9b. The printing results are compared in Fig. 9c and 9d. For molten gallium, the motorized syringe was not able to control the extrusion of the fluid when depositing on the glass substrate, leaving droplets of uncontrollable sizes (Fig. 9c). In contrast, the In-Ga alloy was able to be printed into lines (Fig. 9d). These results indicate that by forming a thixotropic paste, a two-phase alloy may be printed using an extrusion-based 3D printer.





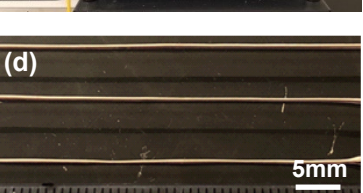


Fig. 9. Thixotropic processing and 3D printing of two testing alloys: (a) phase diagram of In-Ga alloy; (b) syringe-based 3D printer; (c) printed molten gallium metal; (d) manually printed lines from thixotropic 70In-30Ga alloy on glass substrate; (e) manually printed lines from thixotropic 56Bi-44Pb alloy.



In addition, a 56/44 bismuth-lead alloy was also tested. Typically, the bismuth-lead alloy was used as a solder or an easy-handle material for casting. The alloy was heated to 150°C to form a liquid alloy, and then the temperature was reduced. The alloy was vigorously mixed during cooling. A paste-like slurry was formed around 75°C at which the material fluidity was significantly decreased. This thixotropic material was manually printed by movement of a graphite extruder (with 1 mm hole). Line patterns with **sharp tips** (Fig. 9e) were successfully printed.

4.2 Printability study

4.2.1 Effects of nozzle diameter

It should be noticed that all the experiments in this printability study were conducted 4 times for statistically average values. With the steady-state thermal control of the extrusion and printing system, a stable material solid fraction inside the reservoir can be developed. The printing quality resulting from this steady-state system was then evaluated using nozzles with 3 different outlet diameters: 1.5 mm, 1.0 mm, and 0.8 mm. All these printing nozzles were machined as a single piece to mount to the bottom of the reservoir. Throughout the extrusion process, the key process parameters including PID set value, extrusion speed, X-Y platform moving speed, and gap distance between nozzle tip and substrate were maintained (Table 1). The printed lines were measured, and their mean values were used to determine the printing resolution (line width) (Table 2). The comparison of printed lines from nozzles with different sizes is shown in Figure 10.

Table 1. Setup of printing parameters for the test to study the effects of nozzle size.

Printing Parameters	Values
PID set value [°C]	83°C
Extrusion speed [mm/s]	7.87 mm/s
X-Y platform moving speed [mm/s]	4 mm/s
Distance between nozzle tip and substrate [mm]	15 mm

Table 2. Comparison of average (5 times) line width with different nozzle diameter.

Nozzle Diameter [mm]	Average Line Width [mm]	% Difference
1.5	1.85	23.45%
1.0	1.32	32.05%
0.8	1.01	31.21%



Fig. 10. Comparison of printed lines with different sizes of nozzle.

As illustrated in Table 2, a 1.5mm diameter nozzle can extrude a continuous line with a width of 1.85 mm. Under the same conditions, a 1.0 mm nozzle can print lines as thick as 1.32 mm, while a 0.8 mm nozzle can print lines as thin as 0.8 mm. As observed, lines printed by a 1.5 mm nozzle are 23% larger in diameter than their outlet diameter. Lines extruded from 1 mm and 0.8 mm nozzles, on the other hand, are approximately 31% larger than the outlet diameter. From these results, it can be seen that there is a die swell effect in thixotropic printing, and the amount of die swell seems to be dependent on the shear rate. Note that, the shear rate for the 1.5 mm nozzle is the lowest of the three; this may contribute to the reduced amount of die swell. Nevertheless, the nature of the die swell effect in thixotropic extrusion must be studied into detail to uncover the fundamental mechanism. This is beyond the current scope of work but can be incorporated into future work.

4.2.2 Effects of extrusion speed

An electric linear actuator (IP66 series from Progressive Automations) was used in the printing system. The actuator control box allows the extrusion speed to be adjusted between 3.8 and 38.1 mm/s. The actual extrusion speed in the testing experiments was varied between 3.81 and 13.21 mm/s. Other printing parameters are maintained at their default values (Table 3). Straight lines were printed using nozzles with outlet diameters of 1 mm and 1.5 mm. The width of each printed line was measured, and the results are plotted and compared, as in Figure 11.

Table 3. Setup of printing parameters for the test to study the effects of extrusion speed.

Printing Parameters	Values
PID set value [°C]	83°C

Nozzle diameter [mm]	1.5 mm and 1 mm
X-Y platform moving speed [mm/s]	4 mm/s
Distance between nozzle tip and substrate [mm]	15 mm

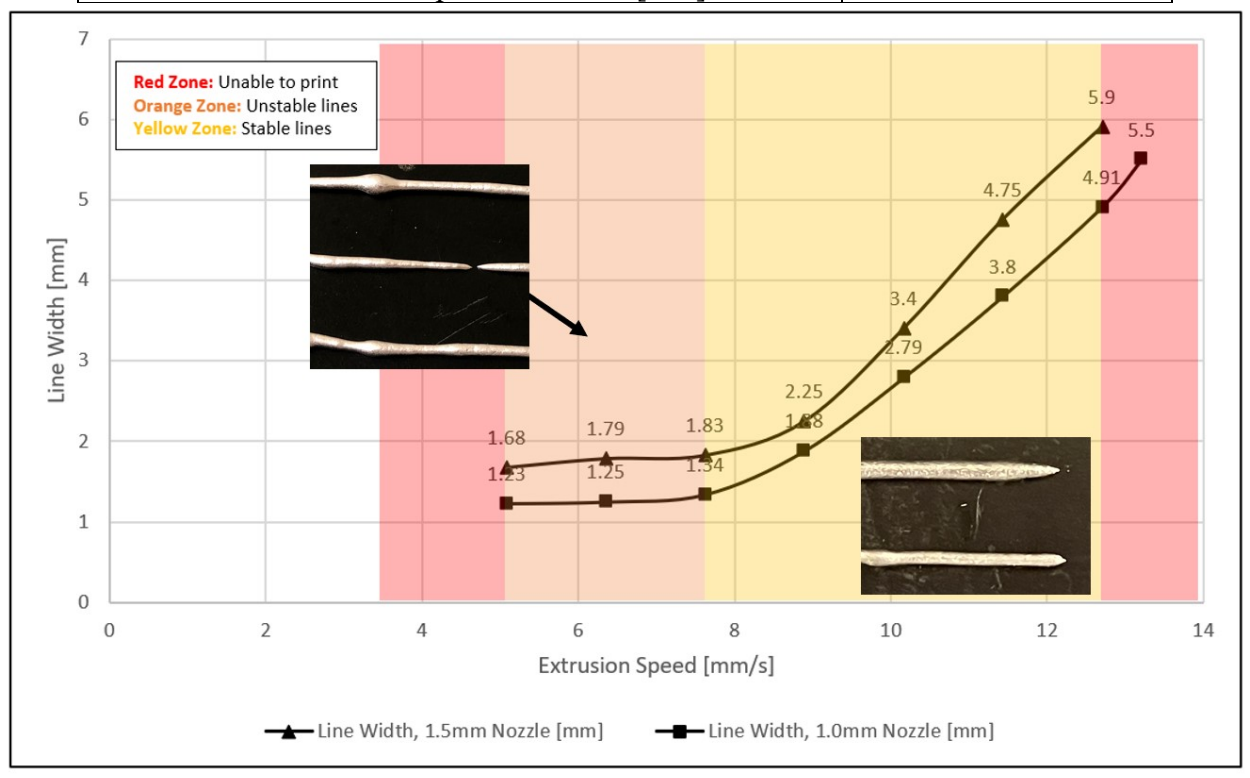


Fig. 11. Illustration of line width under different extrusion speed, both unstable and stable lines are presented in different zones. Two different nozzle diameters are compared: 1.5 mm and 1.0 mm.

As illustrated in Figure 11, both the 1.5 mm and 1.0 mm nozzles were started at a 3.81 mm/s minimum extrusion speed. None of these nozzles, however, can print continuous straight lines at low speeds. Both nozzles can extrude thixotropic alloy on a substrate with a specified length at a rate of 5.08 mm/s, but the printing process was not stable. When the extrusion speed was increased to 6.35 mm/s, the instability issue still remained, and the 1mm nozzle had a higher chance of producing discontinuous lines. Stable measurements were taken at an extrusion speed of approximately 7.62 mm/s. A nozzle with a diameter of 1.5 mm can print a continuous line with an average width of 1.83 mm at this extrusion speed. A 1.0 mm nozzle can produce lines with a width of 1.34 mm at the same speed. Increased extrusion speed resulted in more material being squeezed out of the nozzle tip, which increased the measured line width as well. The final speed recorded in this test was 13.21 mm/s, and both nozzles produced lines with a width of more than 5.5 mm. In particular, with the 1.5 mm diameter nozzle trial, the material flooded out of the outlet at an alarming rate, making it impossible to continue printing lines. Under the same printing conditions, both 1mm and 1.5mm nozzles require enough backpressure and shear rate inside the reservoir to change the thixotropic properties. Therefore, increasing the extrusion speed can instantly raise the shear rate, decreasing the material viscosity. However, when

extrusion speed exceeds the stable printing zone, the thixotropic proprieties are no longer the primary factor to control the material flow rate.

4.2.3 Effect of distance between nozzle tip and X-Y platform

Next, we investigated the effect of the distance between the nozzle tip and the substrate on the printing resolution. Two nozzles with diameters of 1 mm and 1.5 mm were used for comparison purposes. The values of other main process parameters are listed in Table 4. To begin, a 1mm thick gage block was used to determine the distance between the nozzle outlet and platform. The setup distance was initially set to 1 mm and then increased in 1 mm increments. During this test, the maximum distance was 30 mm.

Printing Parameters	Values
PID Set value [°C]	83°C
Nozzle diameter [mm]	1.5 mm and 1 mm
Extrusion speed [mm/s]	7.87 mm/s
X-Y platform moving speed [mm/s]	4 mm/s

Table 4. Printing parameters setup for the test.

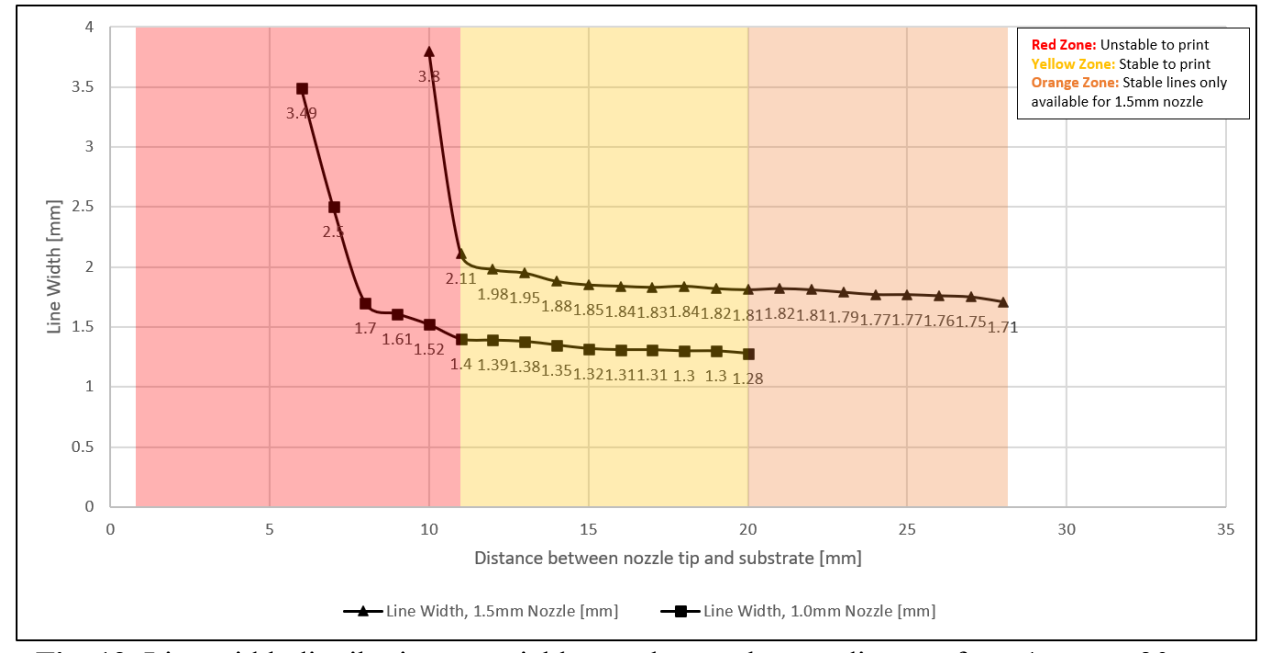


Fig. 12. Line width distribution at variable nozzle-to-substrate distance from 1 mm to 30 mm.

The line widths from different settings were measured and analyzed. Figure 12 shows the distribution of line widths as the distance between the nozzle tip and the platform increased from 1 mm to 30 mm. It is demonstrated that when the gap distance is between 12 and 20 mm, both the two nozzles can produce fine metal lines. If the nozzle is positioned too close to the substrate, material extruded around the nozzle outlet will form a large droplet, which will eventually obstruct the nozzle tip. When the nozzle tip moves out of the blocked area, additional material is dragged out of the droplet, lowering the printing resolution. It was found that a setup distance between 12 and 22 mm produces the best printing results. Line widths for 1.5 mm and 1.0 mm

nozzles varied slightly as distance increased. The 1.5mm nozzle was capable of printing lines up to a distance of 28 mm on the substrate. The 1mm nozzle, on the other hand, can reach a closer distance, but the material does not adhere to the substrate at the 21 mm distance trail.

4.2.4 Effects of X-Y platform moving speed

While the electric linear actuator can produce accurate control of the extrusion speed and can improve printing resolution, the actuator's maximum and minimum movement capabilities limit printing effects. When the extrusion speed is set within a specified range, another significant parameter that can be adjusted is the X-Y platform movement speed. Two motorized linear actuators provide X and Y-axis movement for the printing system. The moving stage's parameters can be configured via CNC control software. Acceleration along both axes was the first parameter considered in this study. Based on the motor movement profile, the CNC control software selected an acceleration value of approximately 50 mm/s². As illustrated in Figure 13(a), when the acceleration was lower than 50 mm/s², a significant amount of material was deposited at the initial point, increasing the risk of the nozzle tip becoming blocked. In contrast, when the acceleration was greater than 50 mm/s², the extruded thread spun, necessitating an extended preparation area to eliminate the spinning lines.

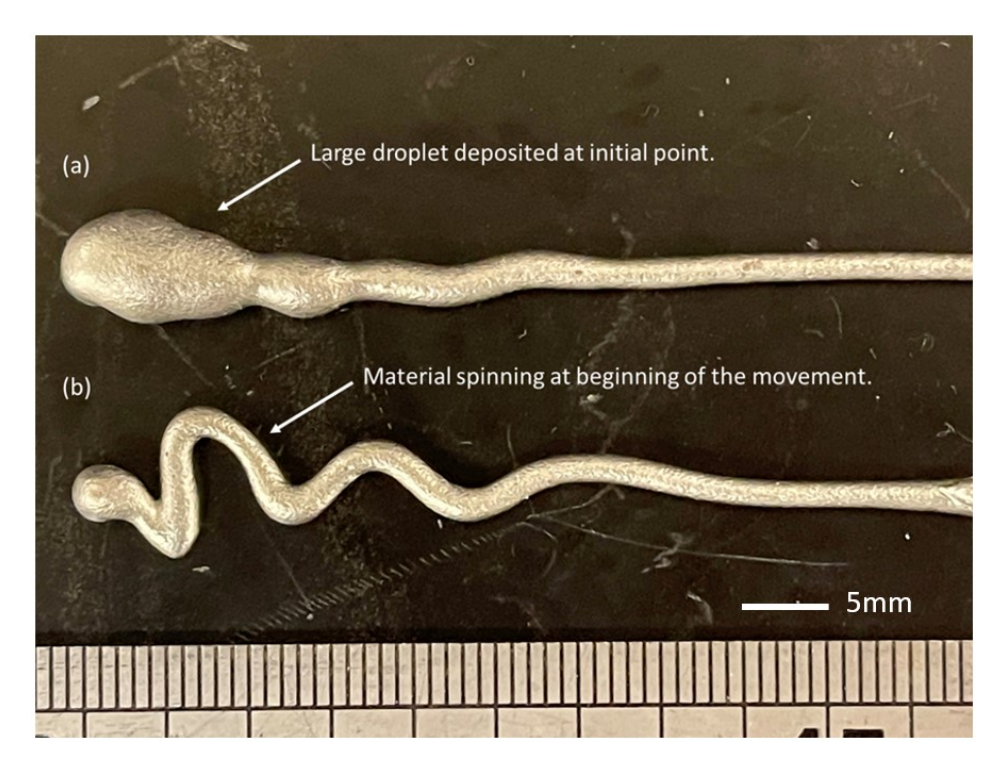


Fig. 13. Extrusion results with different substrate moving acceleration: (a) acceleration lower than 50mm/s² and (b) acceleration higher than 50 mm/s².

The second part of the test was to determine the effect of printing parameters at the same acceleration of on-axis moving speed. As specified in Table 4, the reservoir was heated to 83°C and maintained at that temperature throughout the tests. The distance between nozzle tip and

substrate was set to 15 mm, two nozzles with diameters of 1.5 mm 1.0 mm were compared, and the extrusion speed was set to 7.62 mm/s for the two nozzles.

Table 4. Printing	ng parameters	setup for the	e test.
--------------------------	---------------	---------------	---------

Printing Parameters	Values
PID Set Value [°C]	83°C
Nozzle Diameter [mm]	1.5 mm and 1 mm
Extrusion Speed [mm/s]	7.62 mm/s
Distance between nozzle tip and substrate [mm]	15 mm

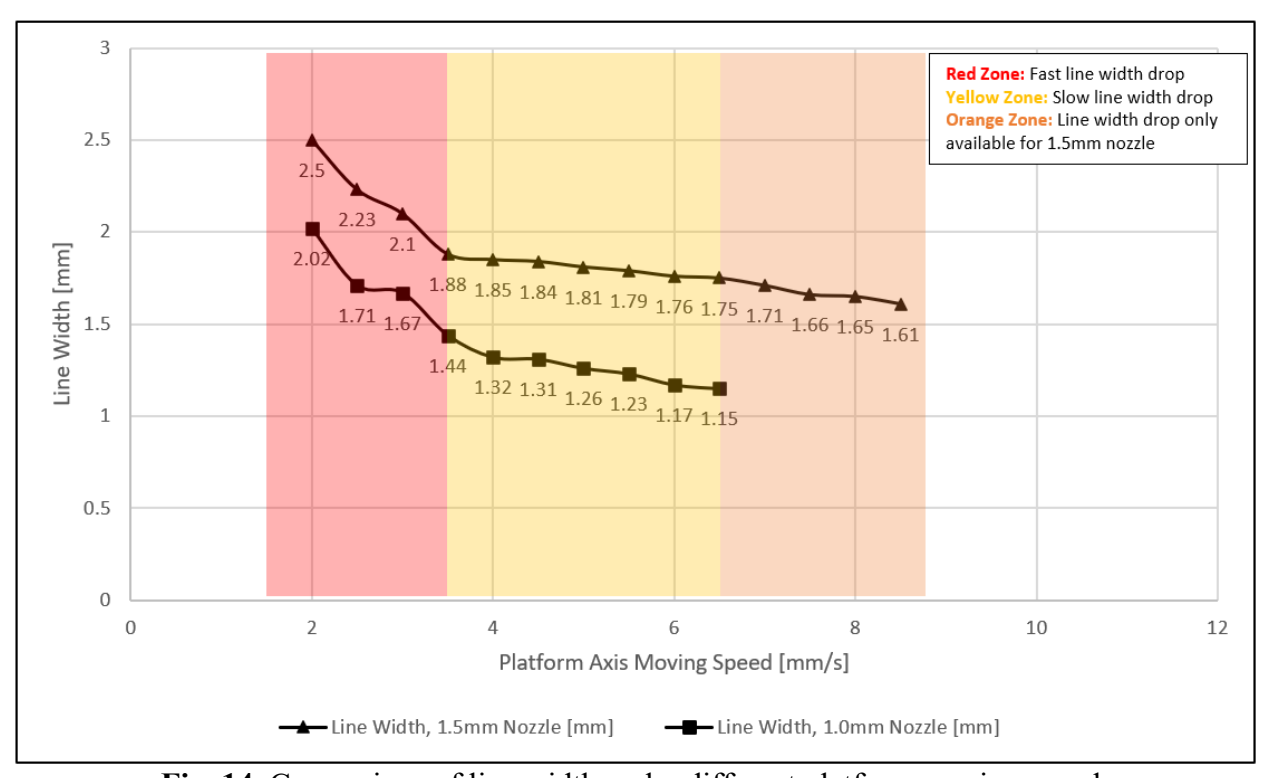


Fig. 14. Comparison of line width under different platform moving speed.

The printed line width with the 1.5mm nozzle reaches an average of 2.5 mm at the slowest moving speed and then decreases dramatically as the moving speed increases to 3.5 mm/s, as shown in Figure 14. When the moving speed is increased from 4 to 8 mm/s, the average line width measured on the substrate decreases gradually until the moving speed exceeds 8.5 mm/s. The results obtained with the 1mm nozzle are consistent with those obtained with the 1.5 mm nozzle trails. The smaller-diameter nozzle, however, showed a limited adjustable moving speed range; discontinuous lines were detected and impacted the print quality at speeds greater than 6.5 mm/s. The best printing resolution for the 1.5 mm nozzle was 1.61 mm, which is 7.33% larger than the initial outlet diameter. Meanwhile, the 1.0mm nozzle can print a line with a width of 1.15 mm, which is 15% wider than the 1.0mm outlet.

4.2.5 Printing results with optimized process parameters

The printability study not only provided us with knowledge on the effects of major process parameters, but also enabled us to optimize the process and create good printing results. For the Bi-Pb alloy, we have accordingly conducted extensive calibration and configuration to develop an optimized printing procedure. The final printing trial with the Bi-Pb alloy was conducted with the following process settings: PID set value to 83°C, actuator extrusion speed to 7.62-7.87mm/s, distance between the nozzle tip and the substrate to 15 mm, nozzle outlet diameters to 1.0 and 1.5 mm, X-Y motion speed to 4mm/s, and X-Y platform acceleration to 50 mm/s². As illustrated in Figure 15c, the thixotropic bismuth alloy was heated to 70.5°C and then extruded through a single-piece nozzle. In Figure 15a and 15b, printed sample lines with nozzles of various diameters are shown. The printing system was examined to demonstrate the entire printing process using a 1.5 mm nozzle. As illustrated in Figure 15d, the printing process included a material preparation step in which heated material was tuned to deposite as a stable line. The nozzle was able to print the desired geometry using CNC software after material preparation.

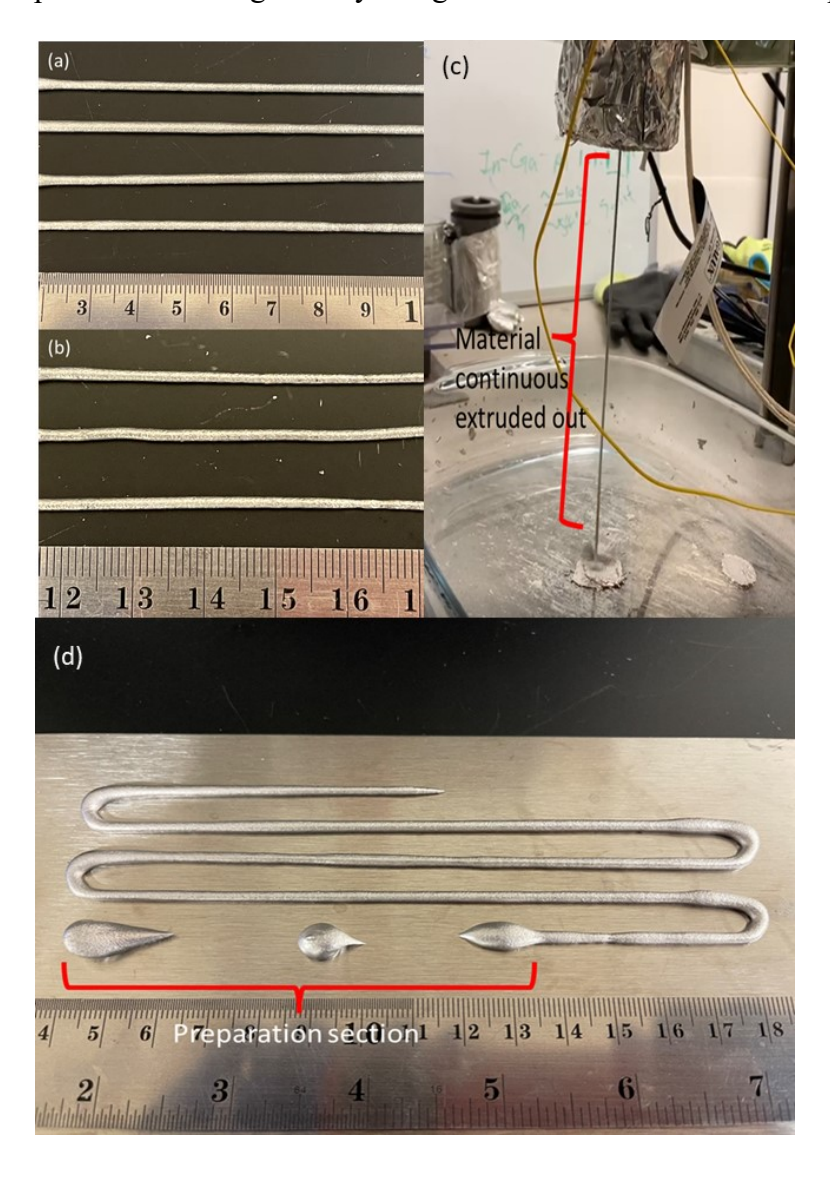


Figure 15. Printed line for (a) 1.5mm diameter nozzle and (b) 1.0mm diameter nozzle. (c)Thixotropic bismuth alloy was extruded out from the reservoir at an extrusion speed of 7.87 mm/s. (d) Printing test for 1.5mm nozzle with zig-zag geometry. The first section of the line was considered as the extruder preparation section, and the material became stable and continuous after this section.

5. Conclusion of the research

From this research it has been demonstrated that metals and alloys may be thixotropically processed and printed by a properly designed extrusion-based 3D printing system, and the thixotropic properties can improve the metal printability. Direct thixotropic metal printing can help optimize the metal printing procedure to reduce post-printing treatments. Thixotropy as a time-dependent property for semi-solid metal processing has been investigated, and the major process parameter on printability has been examined. Low-melting-point alloys were chosen as materials for process demonstration and feasibility study.

An integrated SSM extruder and system was designed and utilized to produce uniform and qualified semi-solid alloy. The SSM extruder was designed to endure the harsh environment in alloy processing convoluted with thermomechanical competing effects. Meanwhile, modulated studies were conducted to understand the functional considerations of individual building blocks in the SSM extruder, for example, a properly designed heating mechanism. The SSM extruder may be used for direct printing or, alternatively, to create thixotropic alloy filaments that may be reheated for printing. In addition, computation simulations were conducted to better understand the dynamics of the process. Simulation results showed that the viscosity and velocity change during processing could significantly affect the dynamics of extrusion. The simulation also assisted in the determination of a temperature profile to create the desired liquid fraction for thixotropic processing.

Parametric studies were also conducted to understand the effects of the major process parameters on the printability during extrusion deposition. Bismuth-based alloy was selected as the testing material for printability study. In particular, the effects of nozzle diameter, extrusion speed, nozzle-to-substrate distance, and platform moving speed and acceleration on the printability were examined. Accordingly, the extrusion and printing system was optimized to achieve desired printing results. The final printing test demonstrated that the integrated system is capable of effectively processing raw alloys in the thixotropic sate and then directly printing by extrusion deposition.

6. Future work

While this research has developed a novel thixotropic material extrusion and printing system for alloys, there a number of studies can be followed for design and process optimization, as well as achieving fundamental understanding of the processing dynamics and principles. Follow-up studies could particularly focus on the following areas. Firstly, the SSM extruder design can be refined and updated. The ideal extrusion system design should produce semi-solid metal filament that can be applied to an FDM printing machine. However, the current auger bit was not suitable for continuous filament extrusion. The material transforming channel can also be redesigned to fit more materials. A material cooling and collecting system is one other desired component of the system. Secondly, the thixotropic printing system can be modified to add gas protection in

order to facilitate processing of a broader range of chemically active metals such as zinc-based and magnesium-based bio-metals. Besides, the extrusion-based printing system resulting from this study was limited by the substrate moving mechanism and extrusion plunger. The extruded material's solidification speed needs to be investigated to determine a suitable degree of rigidity. In addition, local material cooling rate and substrate heating temperature may affect the material rigidity that can support the multiple layer printing. A motorized X-Y-Z moving platform with precision temperature control may improve the printing capability for complex muti-layer geometry printing. Last but not the least, a series of processing-structure-property studies can be performed to better understand the process dynamics/kinetics during thixotropic extrusion and printing. As mentioned earlier, the dynamics of die swell is worth a focused study.

References

- [1] D.H. Hong, D.T. Chou, O.I. Velikokhatnyi, A. Roy, B. Lee, I. Swink, I. Issaev, H.A. Kuhn, P.N. Kumta, Binder-jetting 3D printing and alloy development of new biodegradable Fe-Mn-Ca/Mg alloys, Acta Biomater 45 (2016) 375-386.
- [2] Additive manufacturing general principles terminology, ISO/ASTM 52900, 2015.
- [3] S. Roh, D.P. Parekh, B. Bharti, S.D. Stoyanov, O.D. Velev, 3D printing by multiphase silicone/water capillary inks, Advanced Materials 29(30) (2017) 1701554.
- [4] G.D. Goh, W.Y. Yeong, Mode I interlaminar fracture toughness of additively manufactured carbon fibre thermoplastic, Proceedings of the 3rd international conference on progress in additive manufacturing, 2018, pp. 505-510.
- [5] L.Y. Zhou, J. Fu, Y. He, A review of 3D printing technologies for soft polymer materials, Advanced Functional Materials 30(28) (2020) 2000187.
- [6] Y.Z. Yu, F.J. Liu, R.C. Zhang, J. Liu, Suspension 3D Printing of Liquid Metal into Self-Healing Hydrogel, Adv Mater Technol-Us 2(11) (2017).
- [7] C. Ladd, J.H. So, J. Muth, M.D. Dickey, 3D Printing of Free Standing Liquid Metal Microstructures, Adv Mater 25(36) (2013) 5081-5085.
- [8] S. Hashmi, Comprehensive materials processing, Newnes2014.
- [9] W. Gao, Y.B. Zhang, D. Ramanujan, K. Ramani, Y. Chen, C.B. Williams, C.C.L. Wang, Y.C. Shin, S. Zhang, P.D. Zavattieri, The status, challenges, and future of additive manufacturing in engineering, Comput Aided Design 69 (2015) 65-89.
- [10] G.H. McKinley, M. Renardy, Wolfgang von Ohnesorge, Phys Fluids 23(12) (2011).
- [11] B. Derby, Inkjet Printing of Functional and Structural Materials: Fluid Property Requirements, Feature Stability, and Resolution, Annu Rev Mater Res 40 (2010) 395-414.
- [12] I.D. Joshipura, H.R. Ayers, C. Majidi, M.D. Dickey, Methods to pattern liquid metals, J Mater Chem C 3(16) (2015) 3834-3841.
- [13] D.H. Kirkwood, H.V. Atkinson, K.P. Young, M. Suery, P. Kapranos, SpringerLink (Online service), Semisolid Processing of Alloys, Springer-Verlag Berlin Heidelberg, Berlin, Heidelberg, 2010.
- [14] M.N. Mohammed, M.Z. Omar, M.S. Salleh, K.S. Alhawari, M.A. Abdelgnei, An overview of semi-solid metal processing, Australian Journal of Basic and Applied Sciences 8(19) (2014) 369-373.
- [15] N.H. Husain, A.H. Ahmad, M.M. Rashidi, An overview of thixoforming process, lop Conf Ser-Mat Sci 257 (2017).
- [16] Y. Suh, G. Son, A level-set method for simulation of a thermal inkjet process, Numer Heat Tr B-Fund 54(2) (2008) 138-156.

- [17] S. Simlandi, N. Barman, H. Chattaopadhyay, Behaviour of semisolid slurry flows through a channel, Solid State Phenomena 256 (2016) 146–52.
- [18] R. Koeune, J.-P. Ponthot, A one phase thermomechanical model for the numerical simulation of semi-solid material behavior. Application to thixoforming, International Journal of Plasticity 58 (2014) 120-153.
- [19] M.D. Dickey, R.C. Chiechi, R.J. Larsen, E.A. Weiss, D.A. Weitz, G.M. Whitesides, Eutectic gallium indium (EGaIn): a liquid metal alloy for the formation of stable structures in microchannels at room temperature, Advanced functional materials 18(7) (2008) 1097-1104.
- [20] A. Tabatabai, A. Fassler, C. Usiak, C. Majidi, Liquid-phase gallium-indium alloy electronics with microcontact printing, Langmuir 29(20) (2013) 6194-6200.
- [21] J.W. Boley, E.L. White, G.T.C. Chiu, R.K. Kramer, Direct writing of gallium indium alloy for stretchable electronics, Advanced Functional Materials 24(23) (2014) 3501-3507.
- [22] X.Y. Yin, G.S. Collins, The solubility of indium in liquid gallium supercooled to 12 K, Defect Diffus Forum 323-325 (2012) 503-508.
- [23] B.C. Rugg, T.G. Chart, A Critical-Assessment of Thermodynamic and Phase-Diagram Data for the Gallium-Indium System, Calphad 14(2) (1990) 115-123.
- [24] C.E.T. White, H. Okamoto, Phase diagrams of indium alloys and their engineering applications, ASM International, Metals Park, Ohio, 1992.

Acknowledgement

The authors acknowledge financial support from NSF under Grant No. 2027823 and No. 2027871.